J. Fluid Mech. (1987), *vol.* 184, *pp.* 505–531
Printed in Great Britain

Calculations of edgetone flow with forced longitudinal oscillations

By SAMUEL OHRING

David W. Taylor Naval Ship Research and Development Center,
Bethesda, MD 20084-5000, USA

(Received 3 December 1986 and in revised form 14 April 1987)

Numerical calculations were carried out to study the effect of forced, symmetric, longitudinal flow oscillations on the inherent, strongly antisymmetrical oscillations of a previously studied edgetone flow at a Reynolds number of 450. The flow consists of a two-dimensional jet issuing from a nozzle and impinging on a body with a wedge-shaped leading edge. The flow is assumed to be incompressible, laminar and two-dimensional, and a finite-difference vorticity/stream-function formulation of the Navier–Stokes equations is employed. Three cases were considered with various combinations of forcing frequency and amplitude. It was found that for the two cases with large forcing amplitudes, the naturally dominant flow frequencies lock-in to the forcing frequency and its harmonics. In the third case the forcing amplitude was smaller and lock-in was not observed but the forced oscillations still had a significant impact on the flow. Mode competition between symmetric and antisymmetric modes is discussed for the three cases along with the manner in which the jet vortical structure is altered as a function of time and space. Results for all three cases are presented in the form of computer drawn equivorticity lines and plots of frequency spectra for the jet oscillations and for the pressure on the wedge.

1. Introduction

Recently edgetone flows, which involve the impingement of a planar jet upon an edge, have been studied experimentally in water by Lucas & Rockwell (1984) and computationally, for an incompressible fluid, e.g. water, by Ohring (1986). Earlier, theoretical investigations were performed by Powell (1961).

Experimental investigations have been conducted to study the effects of forcing on free jets. Rockwell (1971) presented a survey of earlier experimental investigations of forced small-amplitude periodic disturbances (typically acoustic) applied to two-dimensional and axisymmetric free jets in both air and water. This survey also included earlier experimental investigations of the unforced edgetone as well as forced attached and reattaching jet flows. It focused on determining the most effective frequency for producing a large-scale change in the mean velocity and fluctuating velocity distributions of the jet.

The survey paper of Ho & Huerre (1984) (hereinafter referred to as HH) presents results for flows involving the forcing (typically acoustic) of a single free shear layer.

Recently, Staubli & Rockwell (1987) experimentally studied the interaction of the planar jet with forced transverse oscillations of the leading edge in the edgetone configuration. They found that the jet oscillations synchronize with the frequency of the controlled edge oscillations for excitation frequencies close to those of the natural jet oscillations.

This paper presents a study of the effect of mechanically forced, symmetric, longitudinal incoming flow oscillations on the inherent, strongly antisymmetrical oscillations of the previous numerically studied edgetone flow at a Reynolds number of 450 described in Ohring (1986) (hereinafter referred to as (O)).

This previously computed unforced edgetone flow (referred to as '$Re = 450$ (from 650)' in (O) and henceforth referred to as the unforced case in this paper) had two major naturally occurring frequencies; one representing the frequency of jet oscillation and the other representing the frequency of vortices shed from each of the jet shear layers.

As in (O), numerical solutions are obtained using a finite-difference vorticity/stream-function formulation of the Navier–Stokes equations. A numerical coordinate transformation is used that maps the physical space coordinates onto computational space coordinates upon which the numerical calculation is performed.

Three cases with various combinations of forcing frequency and amplitude were studied. The results for all three cases are presented in the form of computer drawn and calculated flow vorticity contour lines, and computed spectra for the jet and for pressure at the wedge.

An aim of the present study was to see if the flow for the three cases would lock-in to or be dominated by the forcing frequency with the naturally occurring frequencies being reduced or quenched.

Another aim was to investigate the mode competition expected to result between the forced symmetrical modes and the inherent, antisymmetrical modes of the jet–edge system as well as to investigate the manner in which the jet vortical structure is altered as a function of time and space owing to the forcing for the three cases.

2. Mathematical formulation and numerical method

The mathematical formulation and geometry (figure 1) for the flows considered in this paper are identical with that given in (O) except for several modifications to the boundary conditions, which are described later in this section. The same scaling of the variables is employed here as in (O). The Navier–Stokes equations are written in vorticity–stream-function form and solved using a numerical mapping that maps the physical space coordinates (figure 1*a*) onto a computational space (figure 1*b*) whose coordinates are not shown. The equations are then solved in computational space.

In (O), a steady Couette flow was imposed at the upstream end of the channel (boundary III, figure 1). In this study, the forcing is applied by adding to this Couette flow at the same upstream end of the channel (boundary III in figure 1*a*) a sinusoidally oscillating parallel flow with a prescribed frequency and amplitude.

As the Couette flow is an exact solution of the steady Navier–Stokes equations for parallel flow, the oscillating parallel flow is an exact solution of the corresponding unsteady equations

$$\tilde{u}'_{t'} = \frac{-\tilde{p}'_{x'}}{\rho} + \nu \tilde{u}'_{y'y'} \tag{1}$$

with no-slip boundary conditions at the channel walls,

$$\tilde{u}' = 0 \quad \text{at } y' = \pm \tfrac{1}{2}\delta \tag{2}$$

(δ = channel width). The primes represent dimensional quantities. The constants ρ and ν are the density and kinematic viscosity. The independent variables t', x', y' are time and the horizontal and vertical Cartesian coordinates, respectively. The

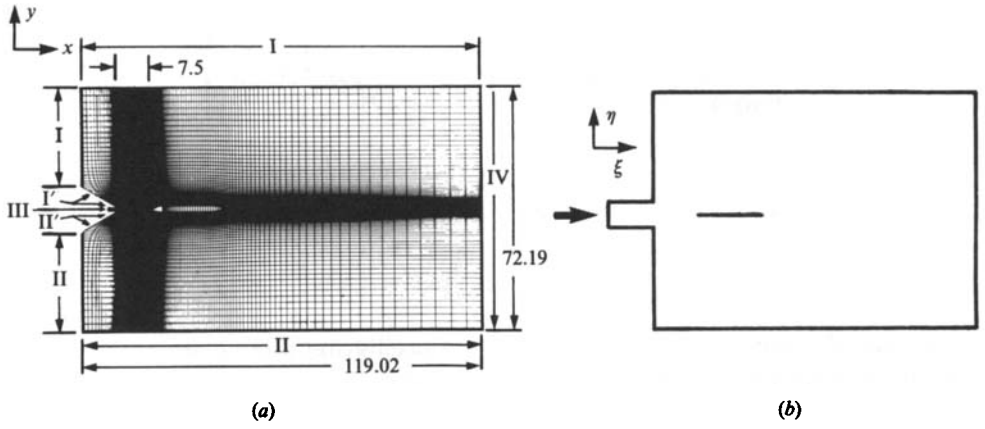

FIGURE 1. Numerical coordinate transformation of physical space coordinate system (*a*) onto computational space (coordinates not shown) (*b*).

dependent variables $\tilde{u}'$, $\tilde{p}'$ are the horizontal velocity and pressure of the oscillating flow.

It is assumed, according to the analogous pipe-flow problem (Schlichting 1968, p. 419), that

$$\frac{-\tilde{p}'_{x'}}{\rho} = A' \exp(imt'), \tag{3}$$

$$\tilde{u}'(y', t') = g(y') \exp(imt'). \tag{4}$$

That is, the flow is assumed to oscillate sinusoidally with prescribed frequency $\tilde{f} = m/(2\pi)$ and amplitude A' (a real number).

Combining (3) and (4) with (1) leads to

$$g_{y'y'} - \frac{img}{\nu} = -\frac{A'}{\nu}. \tag{5}$$

Equations (2) and (4) result in

$$g = 0 \quad \text{at } y' = \pm\tfrac{1}{2}\delta. \tag{6}$$

The solution of (5) and (6) for g is

$$g(y') = -iA' \frac{1 - \cos(y'(-im/\nu)^{\frac{1}{2}})/\cos(\frac{1}{2}\delta(-im/\nu)^{\frac{1}{2}})}{m}. \tag{7}$$

The radical in (7) is evaluated using the principal branch of the logarithm, i.e.

$$\left(\frac{-im}{\nu}\right)^{\frac{1}{2}} = \exp\left\{\frac{1}{2}\left[\ln\frac{m}{\nu} + i(-\tfrac{1}{2}\pi)\right]\right\}$$

$$= \left(\frac{m}{\nu}\right)^{\frac{1}{2}} \exp(-\tfrac{1}{4}i\pi). \tag{8}$$

The real parts of (3) and (4) are retained, since (1) is linear, and the result is

$$\frac{-\tilde{p}'_{x'}}{\rho} = A' \cos(mt'), \tag{9}$$

$$\tilde{u}'(y', t') = G_1(y') \cos(mt') + [A'/m + G_2(y')] \sin(mt'), \tag{10}$$

where
$$G_1(y') = 4A' \frac{[-e_2(y'\alpha)\, e_1(\tfrac{1}{2}\delta\alpha) + e_1(y'\alpha)\, e_2(\tfrac{1}{2}\delta\alpha)]}{mD},$$
$$G_2(y') = 4A' \frac{[-e_1(y'\alpha)\, e_1(\tfrac{1}{2}\delta\alpha) - e_2(y'\alpha)\, e_2(\tfrac{1}{2}\delta\alpha)]}{mD}, \tag{11}$$

and
$$e_1(\zeta) = \cosh(\zeta)\cos(\zeta); \quad e_2(\zeta) = \sinh(\zeta)\sin(\zeta);$$
$$e_3(\zeta) = \cosh(\zeta)\sin(\zeta); \quad e_4(\zeta) = \sinh(\zeta)\cos(\zeta), \tag{12}$$

with
$$\alpha = \left(\frac{m}{2\nu}\right)^{\frac{1}{2}}, \quad D = 4[e_1^2(\tfrac{1}{2}\delta\alpha) + e_2^2(\tfrac{1}{2}\delta\alpha)]. \tag{13}$$

The vorticity $\tilde{\omega}'$ and stream function $\tilde{\psi}'$ for the oscillating forcing are obtained from (10) by differentiation and integration according to

$$\tilde{\omega}'(y', t') = -\tilde{u}'_{y'}(y', t'), \quad \tilde{\psi}'(y', t') = -\int \tilde{u}'(y', t')\, dy' + k. \tag{14}$$

The vorticity $\tilde{\omega}'$ is zero at the centreline, i.e. $\tilde{\omega}'(0, t') = 0$ and the integration constant k is taken to be zero so that $\tilde{\psi}'(0, t') = 0$.

The following non-dimensionalization (identical with that in (0)) is now used:

$$\tilde{\omega}' = \frac{U\tilde{\omega}}{\delta}; \quad \tilde{\psi}' = \delta U\tilde{\psi}; \quad \tilde{u}' = U\tilde{u}; \quad \tilde{p}' = \rho U^2\tilde{p}; \quad Re = \frac{U\delta}{\nu}; \quad St_{os} = \frac{\tilde{f}\delta}{U},$$
$$t' = \frac{\delta t}{U}; \quad (x', y') = \delta(x, y), \tag{15}$$

where Re is the Reynolds number based on the average velocity U of the steady, base (Couette) flow. From the relation $m = 2\pi\tilde{f}$ and (9), (13) and (15) the non-dimensionalization is completed with

$$A' = \frac{AU^2}{\delta}; \quad \alpha y' = y(St_{os}\, Re\, \pi)^{\frac{1}{2}} = y2\gamma; \quad \tfrac{1}{2}\delta\alpha = \gamma; \quad mt' = 2\pi(St_{os})\, t, \tag{16}$$

where A, γ, y and t are non-dimensional.

From (14) and making use of the non-dimensionalization of (15) and (16) in (10)–(13), one obtains the non-dimensional expressions for $\tilde{\psi}(y, t)$, $\tilde{\omega}(y, t)$ and $\tilde{u}(y, t)$:

$$\tilde{\psi}(y, t) = C_1[\{G_5(y) + G_6(y)\}\cos(2\pi St_{os}\, t) + \{-G_3(y) + G_4(y)\}\sin(2\pi St_{os}\, t)] - C_2\, y\sin(2\pi St_{os}\, t); \tag{17}$$

$$\tilde{\omega}(y, t) = C_3[\{-G_3(y) + G_4(y)\}\cos(2\pi St_{os}\, t) + \{-G_5(y) - G_6(y)\}\sin(2\pi St_{os}\, t)]; \tag{18}$$

$$\tilde{u}(y, t) = C_4[G_7(y)\cos(2\pi St_{os}\, t) + G_8(y)\sin(2\pi St_{os}\, t)] + C_2\sin(2\pi St_{os}\, t), \tag{19}$$

for $-\frac{1}{2} \leqslant y \leqslant \frac{1}{2}$, where

$$G_3(y) = [e_3(2\gamma y) + e_4(2\gamma y)]\, e_1(\gamma); \quad G_4(y) = [e_4(2\gamma y) - e_3(2\gamma y)]\, e_2(\gamma);$$
$$G_5(y) = [e_4(2\gamma y) - e_3(2\gamma y)]\, e_1(\gamma); \quad G_6(y) = [e_3(2\gamma y) + e_4(2\gamma y)]\, e_2(\gamma);$$
$$G_7(y) = -e_2(2\gamma y)\, e_1(\gamma) + e_1(2\gamma y)\, e_2(\gamma); \quad G_8(y) = -e_1(2\gamma y)\, e_1(\gamma) - e_2(2\gamma y)\, e_2(\gamma), \tag{20}$$

with non-dimensional constants

$$C_1 = \frac{-A}{2\pi St_{os}\, D\gamma}; \quad C_2 = \frac{A}{2\pi St_{os}}; \quad C_3 = \frac{-4A\gamma}{\pi St_{os}\, D}; \quad C_4 = \frac{2A}{\pi St_{os}\, D}. \tag{21}$$

In (O), the incoming, steady, scaled Couette flow was given by

$$\psi_c(y) = -6y(\tfrac{1}{4}-\tfrac{1}{3}y^2), \quad \omega_c(y) = 12y, \quad u_c(y) = \tfrac{3}{2}-6y^2, \tag{22}$$

for $-\frac{1}{2} \leqslant y \leqslant \frac{1}{2}$ at boundary III. The corresponding constant pressure gradient for the Couette flow was given by

$$p_{cx} = \frac{-12}{Re}. \tag{23}$$

(In (O), the c subscript was dropped.)

The mathematical formulation and geometry (figure 1), for the flows considered in this paper, are identical with that given in (O), except for the following boundary conditions:

$$\left.\begin{aligned}
&\left.\begin{aligned}\psi(y,t;Re,A,St_{os}) &= \psi_c(y)+\tilde{\psi}(y,t;Re,A,St_{os})\\ \omega(y,t;Re,A,St_{os}) &= \omega_c(y)+\tilde{\omega}(y,t;Re,A,St_{os})\end{aligned}\right\} \text{ at boundary III,}\\
&\left.\begin{aligned}\psi(\tfrac{1}{2},t;Re,A,St_{os}) &= \psi_c(\tfrac{1}{2})+\tilde{\psi}(\tfrac{1}{2},t;Re,A,St_{os})\\ &= -\tfrac{1}{2}+\tilde{\psi}(\tfrac{1}{2},t;Re,A,St_{os})\end{aligned}\right\} \text{ at boundaries I', I,}\\
&\left.\begin{aligned}\psi(-\tfrac{1}{2},t;Re,A,St_{os}) &= \psi_c(-\tfrac{1}{2})+\tilde{\psi}(-\tfrac{1}{2},t;Re,A,St_{os})\\ &= \tfrac{1}{2}+\tilde{\psi}(-\tfrac{1}{2},t;Re,A,St_{os})\end{aligned}\right\} \text{ at boundaries II', II.}
\end{aligned}\right\} \tag{24}$$

Notation has been added to indicate dependence on three prescribed flow parameters Re, A and St_{os}.

It is important to know at what times the incoming flow

$$u(y,t;Re,A,St_{os}) = u_c(y)+\tilde{u}(y,t;Re,A,St_{os}) \quad \text{at boundaryIII} \tag{25}$$

achieves its maximum (or minimum) rate.

These times can be found from the relation

$$u_t(0,t;Re,A,St_{os}) = 0, \tag{26}$$

which yields

$$t = \frac{\tan^{-1}[D/4e_2(\gamma)-e_1(\gamma)/e_2(\gamma)]}{2\pi St_{os}} \equiv t_p, \tag{27}$$

where the principal value of the inverse tangent is taken. Then

$$t^* = t_p + k\tfrac{1}{2}T \quad (k \text{ integral}) \tag{28}$$

are the times at which the incoming velocity profile achieves its maximum (or minimum) value at $y = 0$. Here T is the period of the forced oscillations $T = 1/St_{os}$.

The pressure gradient at boundary III (figure 1) is (from (9) and (23))

$$p_x(x,t;Re,A,St_{os}) = p_{cx}+\tilde{p}_x = \frac{-12}{Re} - A\cos(2\pi St_{os}\,t). \tag{29}$$

Integrating (29) from x_0 to x_{III}, where x_{III} is the value of x at boundary III and x_0 is an arbitrary value of x upstream of x_{III}, and then setting $p(x_{III},t;Re,A,St_{os}) = 0$ in this paper, we must have at x_0

$$p(x_0,t;Re,A,St_{os}) = \frac{12(x_{III}-x_0)}{Re} + A\cos(2\pi St_{os}\,t)(x_{III}-x_0). \tag{30}$$

In the laboratory, this value of pressure at $x = x_0$ and time t could be achieved with a pump operating with frequency St_{os}, with A and Re taken into account. The

oscillatory component of the fluid pressure in the flow domain of figure 1 can be interpreted in this way.

The numerical method used in this paper is identical with that used in (O). It should be emphasized that the flow within the channel, including the nozzle opening, as well as the flow in the entire domain of figure 1 (*a*) is computed through numerical solution of the vorticity–stream-function formulation of the Navier–Stokes equations.

3. Numerical results

Three cases were considered in the present numerical study:

(i) $Re = 450, \quad St_{os} = 0.045, \quad A = 0.174;$

(ii) $Re = 450, \quad St_{os} = 0.135, \quad A = 0.174;$

(iii) $Re = 450, \quad St_{os} = 0.135, \quad A = 0.522.$

All three cases have $Re = 450$ and were started abruptly from the case denoted in (O) as $Re = 450$ (from 650) at $t = 204.39$ and then run out to $t = 276.39$. The following results of this section should be compared against the results for $Re = 450$ (from 650) in (O) which had no longitudinal forcing ($A = 0$) and which henceforth will be referred to as the unforced case.

Figure 2 shows computed equivorticity contour-line plots for a typical cycle for this unforced case. In figure 2 and in all the equivorticity contour plots throughout the present paper, equivorticity line values are $\pm 1, \pm 2, \ldots$. Negative equivorticity lines are dashed; positive ones are solid. However in regions of high grid-point density, the dashed lines appear solid. In figure 2 vortices pertinent to the discussion are labelled, and in that figure and throughout the present paper, vortices shed from the jet shear layers, the wedge and the channel lips are defined as regions of vorticity with a local extremum. In figure 2, the jet sways above the wedge with jet shear-layer vortices a, a^{i}, b^{i} from $t = 140.4$ to 148.4. The jet sways below the wedge with vortices a^{ii}, a^{iii}, b^{iii} from $t = 152.4$ to 160.4 at which time a new cycle is starting.

This unforced base case exhibits two major naturally occurring non-dimensional flow frequencies denoted as $\beta = 0.1754$ and $\frac{1}{3}\beta = 0.0585$ in (O) (which were obtained through spectral analysis) with non-dimensional time periods $t_{\beta} = 1/\beta = 5.7$ and $t_{\frac{1}{3}\beta} = 3/\beta = 17.1$, respectively. The frequency $\frac{1}{3}\beta$ represents the frequency of one complete oscillation or flapping of the jet above and below the wedge (occurring every 17.1 time units) and β represents the frequency of vortices shed from either jet shear layer during a complete jet oscillation. The frequency $\frac{1}{3}\beta$ can be viewed as a modulation due to jet shear-layer vortex formation and the subsequent interaction of these jet vortices among themselves and with the wedge, i.e. vortices a, a^{i}, b^{i} at $t = 152.4$ and vortices a^{ii}, a^{iii}, b^{iii} at $t = 160.4$. (Three vortices were shed from either jet shear layer for a total of six vortices shed from both jet shear layers during a complete jet oscillation.) These two major frequencies $\frac{1}{3}\beta$ and β were also found in laboratory experiments (Lucas & Rockwell 1984) using the same geometry as that of figure 1 (*a*) for this Reynolds-number range.

Case (i) was designed to study the effect of an incoming flow oscillation having a frequency St_{os} which is somewhat less (by 23.1 %) than the naturally occurring jet oscillation frequency $\frac{1}{3}\beta$. In particular, it was desired to determine to what extent the overall edgetone flow would 'lock-in' to St_{os}, i.e. to what extent St_{os} and its harmonics (integer multiples of St_{os}) would dominate or even eliminate $\frac{1}{3}\beta$ and its harmonics.

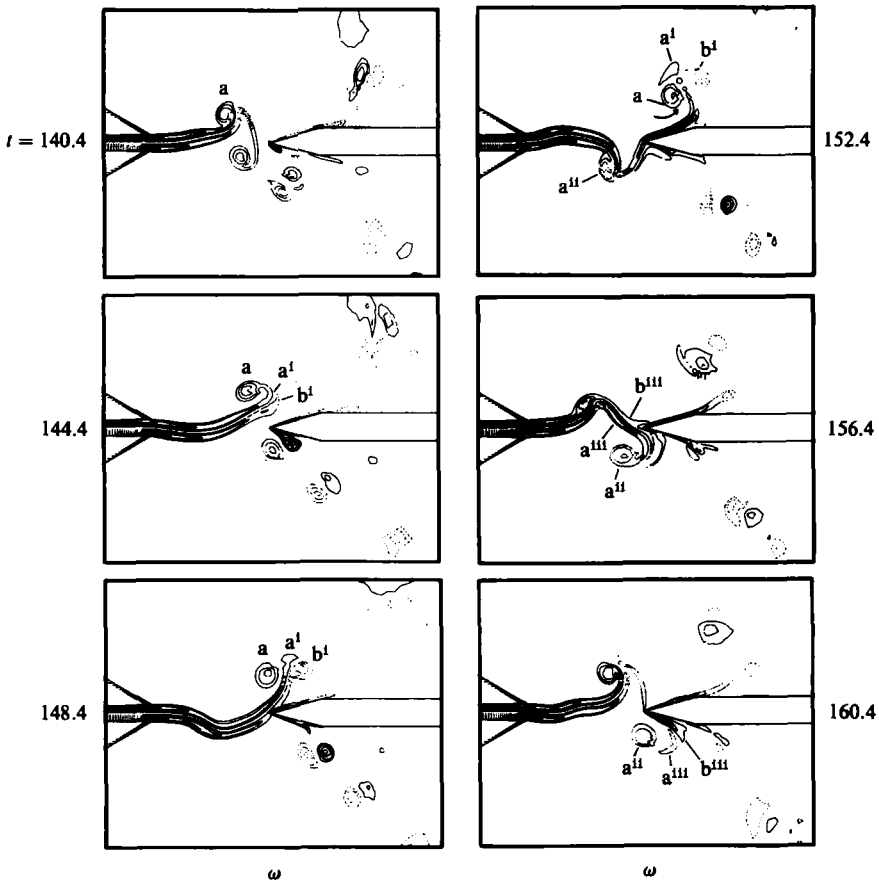

FIGURE 2. Time sequence of vorticity contour plots for a flow cycle for the unforced case (referred to as $Re = 450$ (from 650) in (O)).

Cases (ii) and (iii) were designed to study the effect of an incoming flow oscillation having a frequency St_{os} that is somewhat less (by 23.1 %) than the naturally occurring frequency β. Again it was desired to determine to what extent the overall edgetone flow would lock-in to St_{os}. The amplitude A of the forcing was varied from case (ii) to case (iii) to determine the effect of this parameter on lock-in.

The choices of forcing frequency and amplitude for cases (i)–(iii) were arbitrary in the sense that the threshold values of forcing frequency and amplitude to produce lock-in for cases (i)–(iii) were not known in advance.

However the forcing frequencies St_{os} selected here (compared to the natural frequency β) are analogous to those forcing frequencies f_f (compared to f_n) described in HH for studies of forcing a free single mixing or free single jet shear layer having a natural frequency of vortex formation f_n.

The vorticity dynamics for cases (i), (ii) and (iii) will be compared against that of the unforced edgetone case as regards vortex formation, pairing and amalgamation. This comparison will be guided by the vorticity dynamics of the forced cases of HH. However one should be aware that aside from the nature of the forcing, the edgetone flows considered here involve two jet shear layers that can interact with each other and with the wedge, compared to a single free shear layer emanating from a splitter

plate in HH without any impingement. Also the present paper uses symmetric (about the jet centreline) mechanical forcing compared to the acoustic forcing in HH. Mechanical forcing acts in a more straightforward way in the sense that a large portion of the input energy is converted into instability waves.

Mode competition between the symmetrical modes (due to the forcing) and the inherent, strongly antisymmetrical oscillations of the jet–edge system will also be discussed for cases (i)–(iii).

Figure 3 shows the total incoming velocity profiles (defined by (25) and indicated by arrows) during a complete time period $T = 1/\mathrm{St}_{\mathrm{os}}$ of oscillation for the three cases. The constant Couette velocity profile, used in (O), is included for comparison with the magnitude of the forced longitudinal oscillation at boundary III in figure 1 (*a*). The ordinate from $y = -0.5$ to 0.5 can be thought of as boundary III. The following convention will be adopted in this paper for cases (i)–(iii): for each period T of oscillation, a time variable t_0 is defined in the interval $[0, T]$. The maximum value of the total incoming velocity profile (at $y = 0$) occurs when $t_0 = 0$ and the minimum value of the total incoming velocity profile (at y = 0) occurs when $t_0 = \frac{1}{2}T$. For all t_0 (and t), the incoming velocity profile has a maximum at $y = 0$ (the centre of the channel at boundary III). Thus, in figure 3 (for each case), the incoming flow decelerates from a maximum when $t_0 = 0$ through $t_0 = \frac{1}{4}T$ to $t_0 = \frac{1}{2}T$ when the incoming flow is a minimum. From $t_0 = \frac{1}{2}T$, the incoming flow accelerates through $t_0 = \frac{3}{4}T$ to a maximum at $t_0 = T$. Note that for case (iii), there is actually a small amount of backflow at the walls at boundary III when t_0 is near $\frac{1}{2}T$.

Judging by the amplitudes displayed in figure 3, cases (i) and (iii) would be expected to provide the greatest changes from the unforced case. The results verify this, although, as will be shown, there is substantial change in all three cases. Note that the amplitude of forced oscillation depends on both A and St_{os} as seen from the constants C_2 and C_4 of (21) occurring in (19) for $\tilde{u}(y, t)$ and therefore in (25) for the total incoming flow.

The time $t = 204.39$ when all three cases (i)–(iii) were abruptly started from the unforced case corresponds to $t_0 = 0.943T$, $0.342T$, $0.342T$ for cases (i), (ii) and (iii), respectively.

3.1. *Flow visualizations*

Figures 4, 5 and 6 show computation results in the form of equivorticity lines at times separated by equal intervals for cases (i), (ii) and (iii), respectively. Alongside each equivorticity contour picture values for t_0 are shown as well as for t so that one can refer easily to figure 3 when viewing these contour pictures. The leftmost end of the channel in the contour pictures is boundary III (in figure 1 *a*) where the inflow is specified. In figures 4, 5 and 6 vortices are labelled that are pertinent to the discussion.

Figure 4 shows equivorticity contour pictures for case (i) at times separated by equal intervals of 4.0. The period of the forced incoming flow oscillations is $T = 22.22$. Vortices labelled a, b and c refer respectively to the first, second, and third periods of length T considered.

The first period is considered to start at $t = 220.4$. Then the jet is below the wedge with the vortices $\mathrm{a^i}$–$\mathrm{a^{iii}}$ arranged in a pattern very similar to the unforced edgetone case. These shear-layer vortices, except for $\mathrm{a^i}$, quick dissipate, from $t = 224.4$ to 228.4, before they impinge on the wedge. Meanwhile, at $t = 220.4$, vortex $\mathrm{a^{iv}}$ is forming at the upper channel lip just after the incoming flow has started to increase. For all cases (i)–(iii) vortices form at the channel lips as soon as the incoming flow begins to increase. In addition to the newly formed vortex $\mathrm{a^{iv}}$, new vortices $\mathrm{a^v}$ and $\mathrm{a^{vi}}$ have formed in the jet at $t = 224.4$ and $\mathrm{a^{vii}}$ has formed at $t = 228.4$. The jet sways

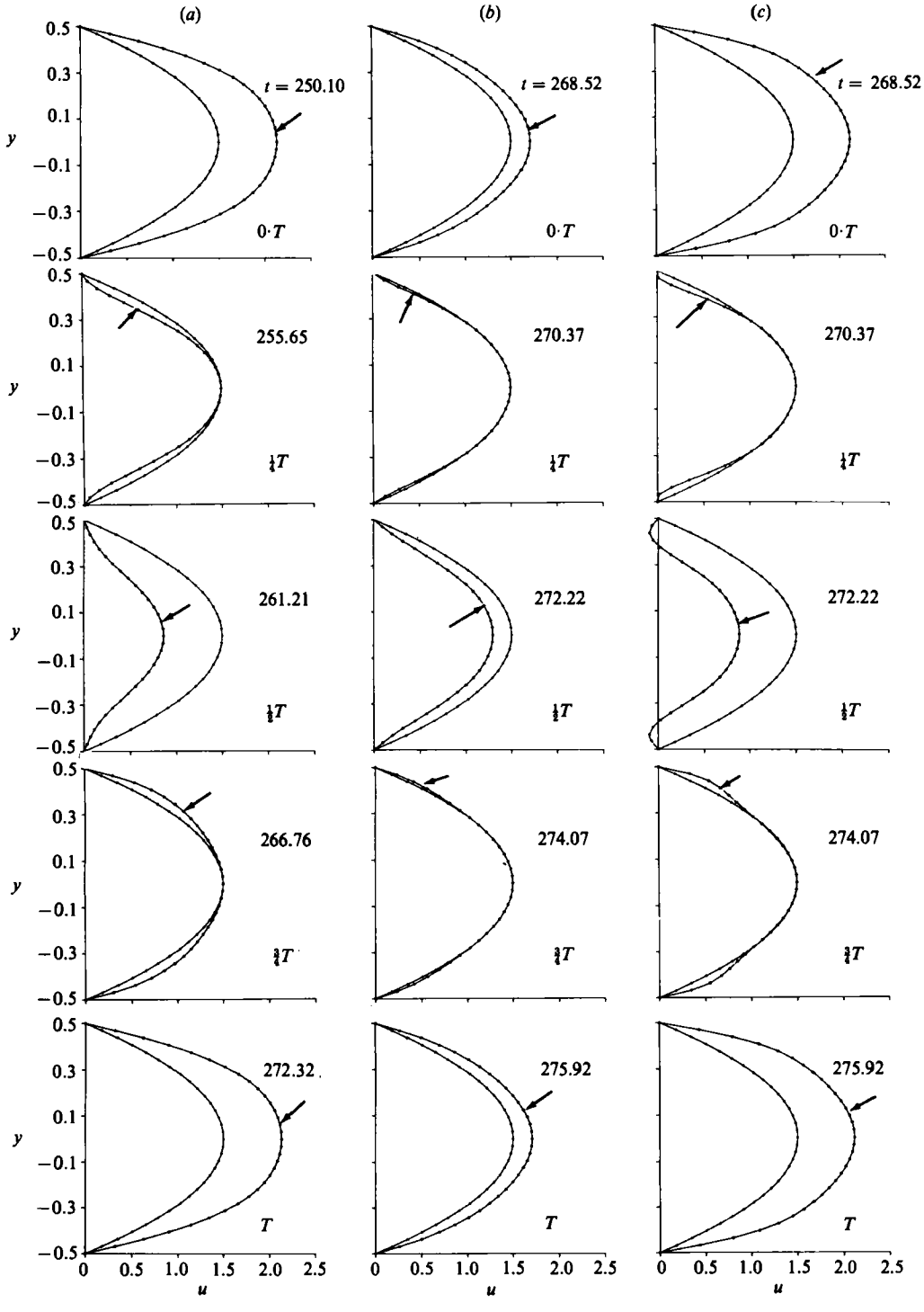

FIGURE 3. Total incoming horizontal velocity profiles (indicated by arrows) during a complete time period T of forced oscillation for (*a*) $St_{os} = 0.045$, $A = 0.174$, (*b*) $St_{os} = 0.135$, $A = 0.174$ and (*c*) $St_{os} = 0.135$, $A = 0.522$. The constant Couette velocity profile used in (O) is shown for comparison. The corresponding values t and t_0 are shown near the top and bottom, respectively, of each velocity profile graph.

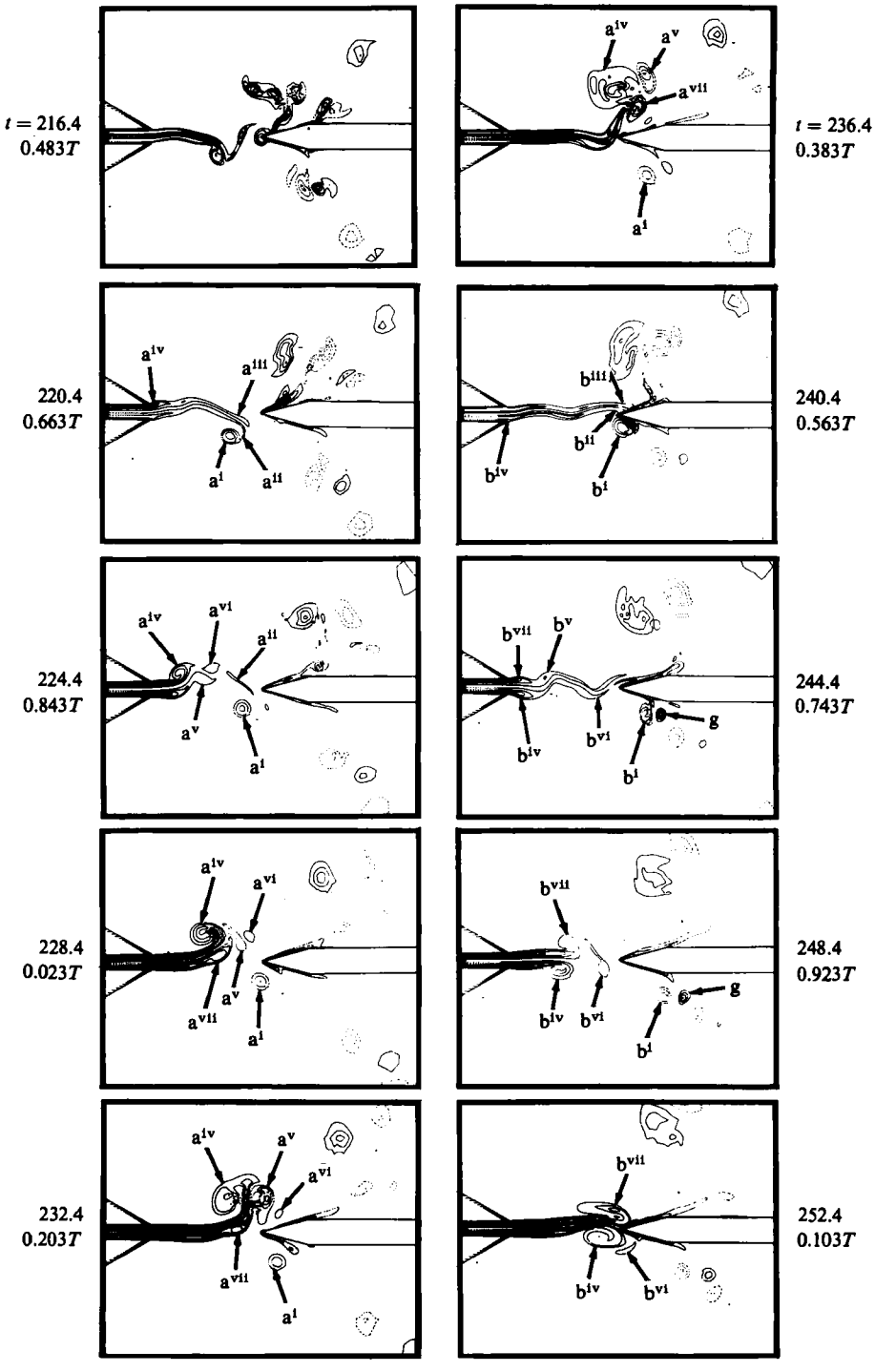

FIGURE 4. For caption see facing page.

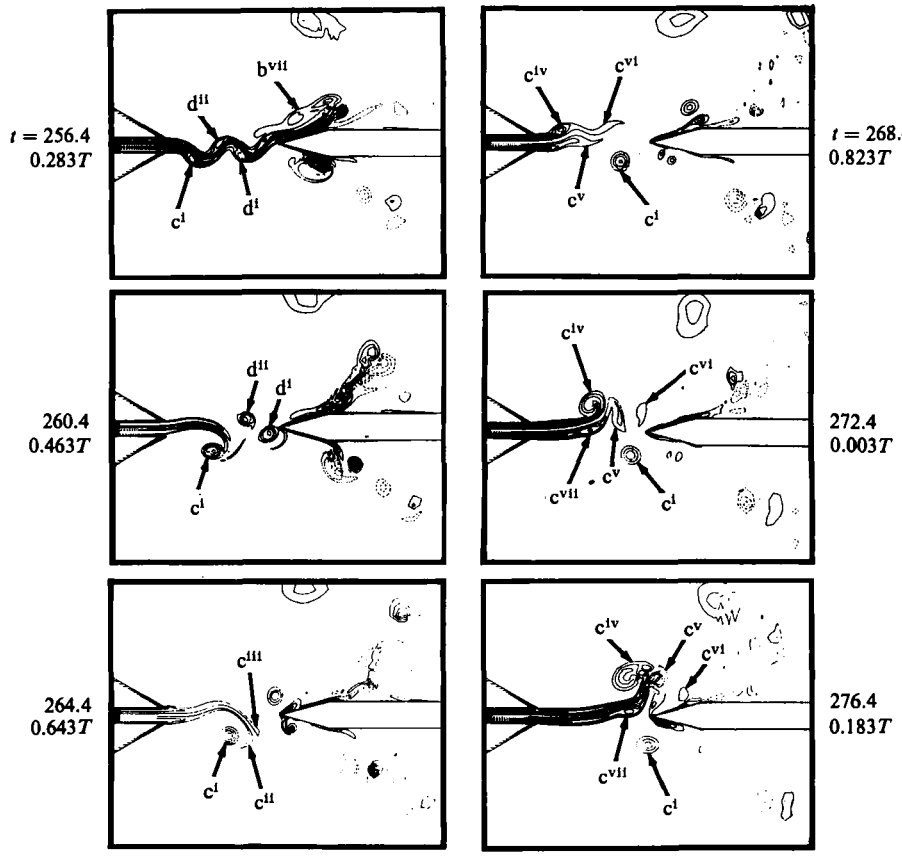

FIGURE 4. Time sequence of vorticity contour plots for $St_{os} = 0.045$, $A = 0.174$.

to the upper side of the wedge during the interval between $t = 224.4$ and 236.4. The jet impinges on the wedge at $t = 236.4$ with vortices a^{iv}, a^{v} and a^{vii} arranged in a pattern closely resembling that of the unforced edgetone case. The jet then completes its oscillation cycle when it sways below the wedge and impinges at $t = 240.4$ with vortices b^{i}, b^{ii} and b^{iii}. At $t = 240.4$, vortex b^{i} is inducing a vortex g of opposite sign at the wedge and the vortex pair b^{i}–g can then be seen 'shooting off' the wedge at $t = 244.4$, and later times. This process has been observed in (O) and by Lucas & Rockwell (1984) and can be seen to occur for cases (i)–(iii) throughout figures 4, 5 and 6.

At $t = 240.4$, the second time period of length T is starting with vortex b^{iv} forming at the lower channel lip at a time when the incoming flow has just started to increase. (The a, b and c vortices have been similarly numbered to show correspondence between the cycles.) The jet sways slightly above the wedge and impinges head-on at the wedge at $t = 252.4$. At $t = 256.4$, with the incoming flow decelerating (decreasing), the jet is quite unstable with two extra vortices d^{i} and d^{ii}. This type of destabilization did not occur during the other computed time intervals when the incoming flow is decelerating (decreasing) (i.e. when t is in the intervals [228.4, 236.4] and [272.4, 276.4]). In fact, during these time intervals, the jet vortices grow considerably and the jet stem lengthens. The jet then completes its oscillation cycle with the jet below the wedge at $t = 264.4$ with vortices c^{i}, c^{ii} and c^{iii}. The third cycle

bears a striking resemblance to the first cycle, i.e. compare the time interval $t = 264.4$ to 276.4 with the time interval $t = 220.4$ to 232.4. These time intervals are extremely close to being $2T$ apart.

To summarize for case (i):

1. The major frequency of the flow for case (i), which is the frequency for one complete oscillation or flapping of the jet, is $St_{os} = 0.045$ (the frequency of the incoming flow oscillation). The period of oscillation is thus $T \approx 22.22$, an increase from $t_{\frac{1}{3}\beta} = 17.1$ for the non-forced case. The jet oscillation for case (i) bears a resemblance to that of the unforced case except that (*a*) the jet oscillation frequency has been changed and locked into $St_{os} = 0.045$, and (*b*) there appear to be seven jet vortices per jet oscillation. These results will be borne out by the spectral analysis presented later in the paper which will also show the subjugation of the naturally occurring frequency $\frac{1}{3}\beta$ (and its harmonics) of the unforced case to the frequency $St_{os} = 0.045$. One can indeed say that lock-in has occurred for case (i).

2. Compared to the unforced edgetone case, case (i) shows (*a*) earlier formation of jet shear-layer vortices, i.e. vortices a^{iv}, b^{iv} and c^{iv} at $t = 220.4$, 244.4 and 268.4, respectively, (*b*) earlier (further upstream) development of larger vortices, i.e. vortices a^{iv}, b^{iv} and c^{iv} at $t = 232.4$, 252.4 and 276.4, respectively, (*c*) earlier pairing of vortices, i.e. vortices a^{iv}, a^{vii} and vortices c^{iv}, c^{vii} at $t = 228.4$ and 272.4, respectively and (*d*) earlier and larger promotion of vortex amalgamation and merging as for vortices a^{iv}, a^{v} and a^{vii} at $t = 232.4$, 236.4 and vortices c^{iv}, c^{v} and c^{vii} at $t = 272.4$, 276.4. These results are analogous with those of the low-forcing-frequency cases of HH. Case (i) has a low forcing frequency $St_{os} < \frac{1}{3}\beta$ and a large forcing amplitude of oscillation which can be compared against analogous low-frequency-forcing cases in HH with $f_f < \frac{1}{3}f_n$. These low-forced-frequency cases in HH promoted multiple-vortex amalgamations and tended to shift vortex pairing upstream. Furthermore, by increasing the forcing level, the formation of the large vortices was shifted upstream.

3. The inherent, strongly antisymmetrical oscillations of the jet–edge system apparently overtakes the forced symmetric mode not far downstream from the channel opening. The symmetric mode appears to dominate near the channel opening, i.e. at $t = 224.4$, 244.4, 248.4 and 268.4.

4. The flow for case (i) is clearly periodic as is easily seen in figure 4, e.g. by comparing the flow at $t = 232.4$ with that at $t = 276.4$. However the flow is biased in the sense that the very large vortex amalgamations occur above the wedge during the few cycles shown in figure 4. This may very likely be due to the greater abruptness of the start (compared to cases (ii) and (iii)) from the unforced case at a time corresponding to $t_0 = 0.943T$ when the symmetric incoming longitudinal flow oscillation at boundary III (figure 1 a) is almost a maximum (see figure 3). Presumably if many flow cycles could be computed, the flow would approach an unbiased equilibrium. Owing to computer expense this is not possible at the present time.

Figure 5 shows equivorticity contour pictures for a typical flow cycle for case (ii) at times separated by intervals of 2.0 (in contrast to 4.0 for case (i)). For case (ii) the time period for the forced incoming flow oscillation is $T = 7.41$ and the amplitude of oscillation is the smallest of the three cases considered (see figure 3).

From $t = 230.4$ to 238.4, vortices a^{i}, a^{ii} and a^{iii} are shed from the jet shear layers and these vortices impinge on the wedge from $t = 238.4$ to 240.4. (Vortices such as d^{i} at $t = 232.4$ and d^{ii} at $t = 236.4$ are weak and dissipate very rapidly compared to the a vortices in figure 5 and will not be part of the discussion.) New vortices a^{iv}, a^{v} and a^{vi} are shed from the jet shear layers from $t = 240.4$ to 246.4 with the vortices a^{iv} and a^{v} impinging on the wedge at $t = 248.4$. At $t = 248.4$ a new cycle is beginning

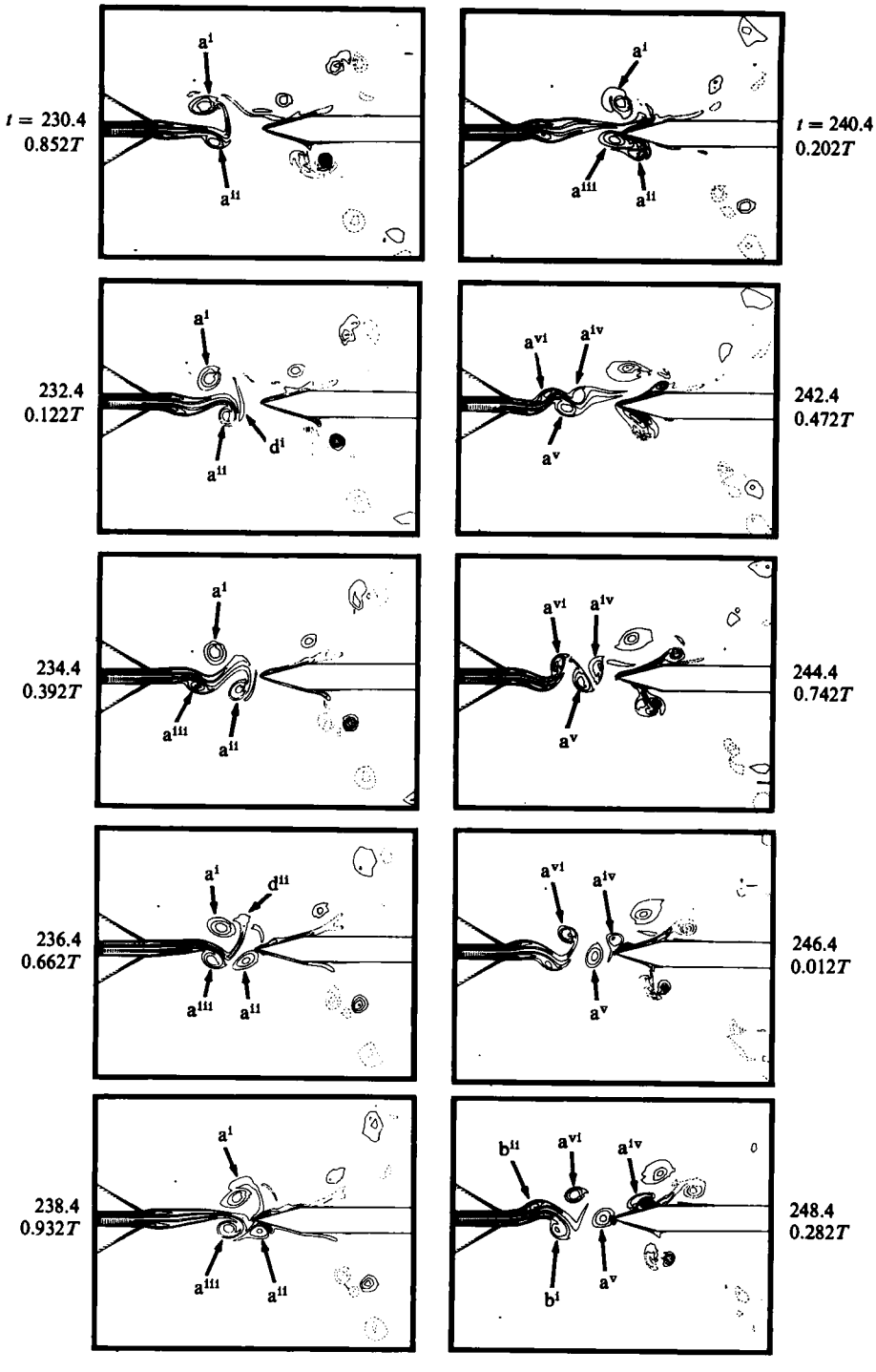

FIGURE 5. Time sequence of vorticity contour plots for a flow cycle for $St_{os} = 0.135$, $A = 0.174$.

with vortices b^{i} and b^{ii} being shed from the jet. The cycle referred to is approximately 18 time units long which is close to the time period $t_{\frac{1}{3}\beta} = 17.1$ for one complete naturally occurring oscillation of the jet for the unforced case. Thus the fundamental frequency of the non-forced case is little affected by the forcing of case (ii). Spectral analysis presented below will show $\frac{1}{3}\beta$ to be one of the dominant frequencies for case (ii).

Impingement of the jet vortices on the wedge occurs at times $t = 240.4$ and 248.4, or approximately at intervals of $t_{\frac{2}{3}\beta} = 8.55$ which is the time required for one-half of a naturally occurring complete jet oscillation and thus impingement for the unforced case.

One of the striking features of case (ii) is the frequency of the vortices shed from the jet shear layers. Three vortices are shed per impingement or six vortices are shed from the jet shear layers approximately every $t_{\frac{1}{3}\beta}$ so that the frequency of vortices shed from either shear layer is β. Spectral analysis presented below will show that $\beta = 0.1754$, which is also very nearly equal to $\frac{4}{3}St_{os} = 0.18$, is the dominant frequency of the flow for case (ii) along a substantial portion of the jet. The frequency β was the second most dominant frequency (after $\frac{1}{3}\beta$) for the unforced case.

During times of decelerating (decreasing) incoming flow, the jet is especially unstable with vortices shed at times $t = 232.4$, 234.4, 240.4, 242.4, 246.4, 248.4, etc., i.e. when t_0 is in $(0, \frac{1}{2}T)$. During times of accelerating (increasing) incoming flow, the jet lengthens as seen at $t = 230.4$, 236.4, 238.4, etc., i.e. when t_0 is in $[\frac{1}{2}T, T]$.

Based on the flow visualization in figure 5, case (ii) flow has not locked-in to the frequency $St_{os} = 0.135$ of the incoming flow although case (ii) flow has some substantial differences compared to the unforced case.

To summarize for case (ii):

1. Case (ii) flow is similar to the unforced case in the following important respects: (*a*) case (ii) has dominant frequencies β, $\frac{1}{3}\beta$, $\frac{2}{3}\beta$ and (*b*) impingements occur with frequency $\frac{2}{3}\beta$.

2. Case (ii) flow differs from the unforced case in the following important respects: (*a*) jet shear-layer vortices are stronger and are shed further upstream nearer to the channel nozzle, (*b*) the swaying of the jet is not easily discernible as the length of the jet stem varies considerably at different times, and (*c*) β is a more dominant frequency.

3. The formation of jet vortices further upstream compared to the unforced case is consistent with analogous results for forcing cases mentioned in HH for a single free shear layer when $f_f \approx f_n$ and the forcing level (or amplitude) is raised. (Case (ii) has $\frac{3}{4}\beta < St_{os}$ analogous to f_f and β analogous to f_n, i.e. $\frac{3}{4}\beta < St_{os} \approx \beta$.) As mentioned in HH, shear-layer vortices form further upstream as the forcing level is raised for these cases.

4. The level of forcing amplitude for case (ii) is not great enough for the forced symmetric mode to dominate the inherent, strongly antisymmetrical oscillations of the jet–edge system except for a weak hint of dominance very close to the channel opening, i.e. at $t = 230.4$, 232.4, 238.4 and 240.4.

Figure 6 shows equivorticity line pictures for a typical flow cycle for case (iii) at times separated by intervals of 2.0. Case (iii) differs from case (ii) only in that the incoming flow has a greater amplitude of oscillation (see figure 3).

At $t = 238.4$, vortices a^{i}, a^{ii} and a^{iii} have already been shed. The intense vortices a^{i} and a^{ii} of approximately equal strength were shed from the nozzle lips during $\frac{1}{2}T < t_0 < T$, when the incoming flow is increasing, while vortex a^{iii} has been shed from the jet further downstream. Vortices a^{i} and a^{ii} grew as they were convected

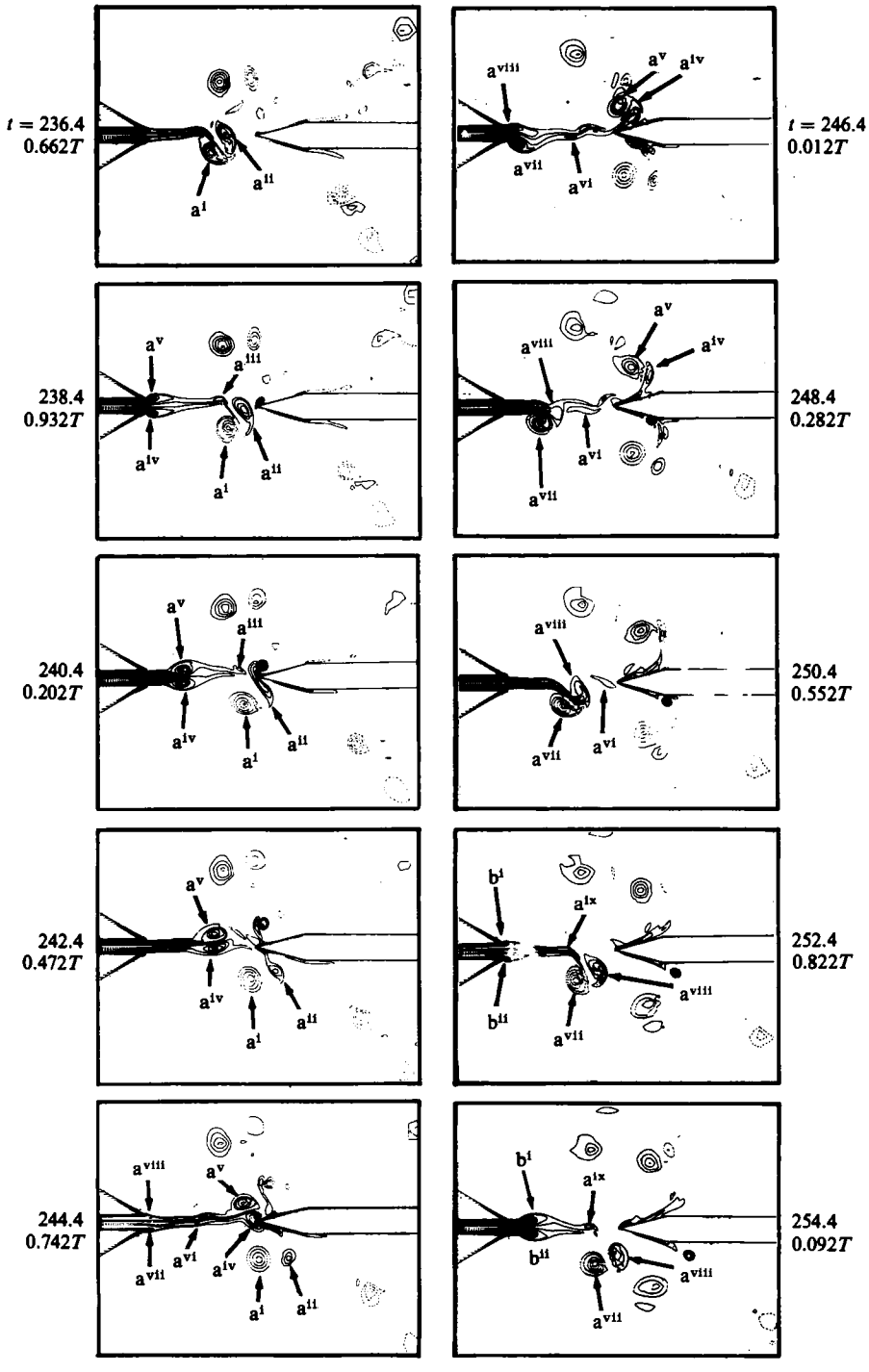

FIGURE 6. Time sequence of vorticity contour plots for a flow cycle for $St_{os} = 0.135$, $A = 0.522$.

downstream. At $t = 238.4$, vortices a^{i} and a^{ii} together with a^{iii} give the appearance of a jet that is swaying below the wedge at $t = 238.4$ before impinging at $t = 240.4$. Meanwhile at $t = 240.4$, new vortices a^{iv} and a^{v}, of approximately equal strength, which previously shed from the nozzle lips during $\frac{1}{2}T < t_0 < T$, are growing as they are convected downstream. The jet with vortices a^{iv}, a^{v} and a^{vi} sways above and then impinges on the wedge at $t = 244.4$. At this time, newly shed vortices a^{vii}, a^{viii} from the nozzle lips start to grow and move downstream. The jet, with vortices a^{vii}, a^{viii} and a^{ix}, then sways below the wedge at 254.4 completing the cycle.

To summarize for case (iii):

1. The entire jet appears to be flapping, or oscillating, with a frequency approximately equal to $\frac{1}{2}St_{os}$, i.e. the time period of the jet oscillation is approximately $2T = 14.82$. This period can be verified with the comparison of pictures at $t = 238.4$ and 254.4.

2. The jet appears to be impinging at the wedge with frequency St_{os}, i.e. the time period of impingement is approximately $T = 7.41$. This period can be seen best by comparing pictures at $t = 238.4$ and 246.4.

3. A total of six vortices form along the jet during each time interval of length $2T = 14.82$. Three vortices are shed from each side of the jet during each such interval which yields another dominant frequency, for individual vortex formation, of $\frac{3}{2}St_{os}$.

4. The prior observations and other data presented later provide strong evidence that case (iii) flow has locked-in to the dominant frequencies $\frac{1}{2}St_{os}$, St_{os} and $\frac{3}{2}St_{os}$. The natural jet oscillation time period $t_{\frac{1}{2}\beta}$ of the unforced case has been shortened to $2T$ under the influence of the large-amplitude forced oscillation of the incoming flow.

5. Case (ii) flow with its smaller amplitude for the same forced frequency St_{os} appears to be a transitional case between the unforced case and case (iii) flow.

6. Vortices that are shed from the channel lips during case (iii) flow are more intense than any vortices that are shed from the jet during case (ii) flow. The increased forcing level of case (iii) compared to case (ii) flow causes earlier and more intense jet vortex formation to occur right at the channel lips when compared to case (ii). This is consistent with the analogous forcing cases of HH with $f_f \approx f_n$ when the forcing level is raised. (Case (iii) flow has a forced frequency St_{os} such that $\frac{3}{4}\beta < St_{os} \approx \beta$.)

7. The forced symmetric mode appears to dominate over the inherent antisymmetrical oscillations of the jet–edge system for a considerable length downstream from the channel opening. This is especially noticeable at times $t = 240.4$, 242.4, 244.4, 252.4 and 254.4.

The following general remarks can be made about cases (i)–(iii) based on the previous discussion:

(*a*) Lock-in of the jet–edge system to the forcing frequency St_{os} is achieved at both the lower and higher forcing frequencies of cases (i) and (iii), respectively, owing to the high level of forcing. Lock-in of the jet–edge system to the higher forcing frequency of case (ii) is not achieved because of the relatively low level of forcing used (see figure 3).

(*b*) For cases (i)–(iii) an oscillating or 'flapping' jet is preserved in the jet–edge system despite the forcing although the jet structure itself varies considerably among the three cases.

(*c*) Earlier (further upstream) vortex formation, pairing and amalgamation occurs at the lower-forcing-frequency, high-forcing-level case (i) compared to the unforced case. In addition, the higher-forcing-frequency cases (ii) and (iii) also cause earlier jet vortex development compared to the unforced case with the earliest development occurring for the higher-forcing-level case (iii). These results agree with the analogous

forcing cases in HH where the forcing was applied to a free shear layer emanating from a splitter plate.

(*d*) The high forcing level of cases (i) and (iii) causes the forced symmetric mode to dominate over the inherent, strongly antisymmetrical oscillations of the jet–edge system near the channel opening. For case (iii), the symmetric mode domination extends a considerable distance downstream of the channel opening. No such symmetric domination exists for the lower forcing level of case (ii).

3.2. *Numerical spectral results along the jet*

Figure 7 shows, for the unforced case, the growth of spectral-component amplitudes along the jet centreline ($y = 0$) for the transverse velocity (v velocity component). Note that $\frac{1}{3}\beta$ and β are dominant. The harmonics of $\frac{1}{3}\beta$ that are shown are essentially those components that are greater than 10% of the maximum for a measurable distance along the jet. $L = 7.5$ is the non-dimensional distance from the nozzle opening to the wedge tip. All distances have been scaled by the width of the channel. Figure 7 should be compared with figures 8, 9 and 10 for cases (i), (ii) and (iii), respectively.

Cases (i)–(iii) occur from time $t = 204.39$ to 276.39. Therefore it was convenient to apply the Fourier analysis for all functional time histories considered in this paper to a time interval from $t = 209.99$ to 276.39, which is 66.4 time units long. This time interval is very close to 66.66, which is three periods of the imposed flow oscillations for case (i) and nine periods for cases (ii) and (iii). Values were recorded during this time interval at 166 uniformly spaced time levels. The Fourier analysis has been applied directly to the numerical data from the flow solution in the same manner as in (O). Filtering of the numerical data is avoided and is not justified because only a few flow cycles are available for the Fourier analysis due to the present expense of flow computation.

Figure 8 (*a–c*) shows, for case (i), the pertinent spectral-component amplitudes $A_{\tilde{v}}$ for the transverse velocity v plotted versus x/L (from 0 to 1.0) along the jet centreline. (The spectral component amplitudes for all time histories in this paper are as defined in (O).) All spectral components that are not essentially zero have been considered in figure 8 (*a–c*) where the ordinates are of log type. Figure 8 (*a*) shows the spectral components for the frequency St_{os} and its superharmonics whereas figure 8 (*b*) shows components for $\frac{1}{3}\beta$ and its superharmonics. Figure 8 (*c*) shows all other non-zero components. For all cases (i)–(iii), the extra energy input into the flow due to the mechanically forced longitudinal oscillations produces a significant increase in the number of non-zero spectral components well beyond that for the corresponding unforced edgetone flow as seen in figure 7. This increase in spectral components is significantly larger than the increase of spectral components that might be expected to result from acoustical forcing. Because a large number of computed flow cycles are not available in the present paper for each of the cases (i), (ii) and (iii), owing to the computer expense of flow computation, the Fourier analysis cannot be expected to resolve the additional increase of spectral components as well as if additional flow cycles were available.

From figure 8 (*a–c*) it is clear that the St_{os} component dominates all other components, which is in agreement with the previous discussion of the vorticity field. The dominance of St_{os} is for the entire distance between channel nozzle and wedge tip (from $x/L = 0$ to 1.0). The shape of the curve for the St_{os} component in figure 8 (*a*) strongly resembles the curve for the $\frac{1}{3}\beta$ component for the unforced case (see figure 7). The shape of the $\frac{1}{3}\beta$ curve for the unforced case was also verified in the

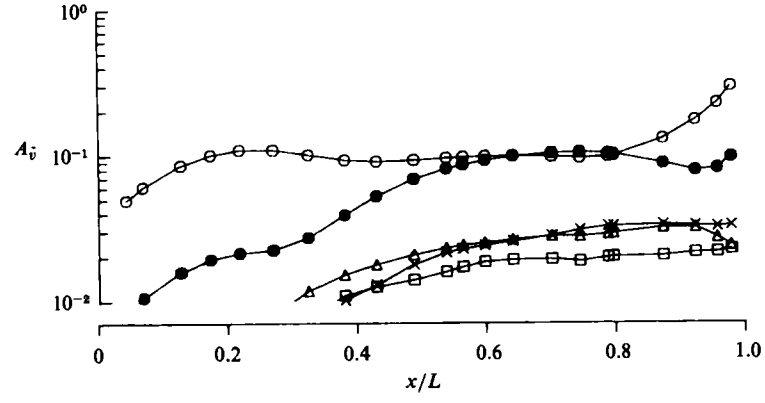

FIGURE 7. Growth of spectral-component amplitudes of the transverse velocity v along the jet centreline ($y = 0$) for the unforced case. The components are: ⬡, $\frac{1}{3}\beta$; △, $\frac{2}{3}\beta$; ⬢, β; ×, $\frac{4}{3}\beta$; □, $\frac{5}{3}\beta$. (Graph vertical ordinates of log type.)

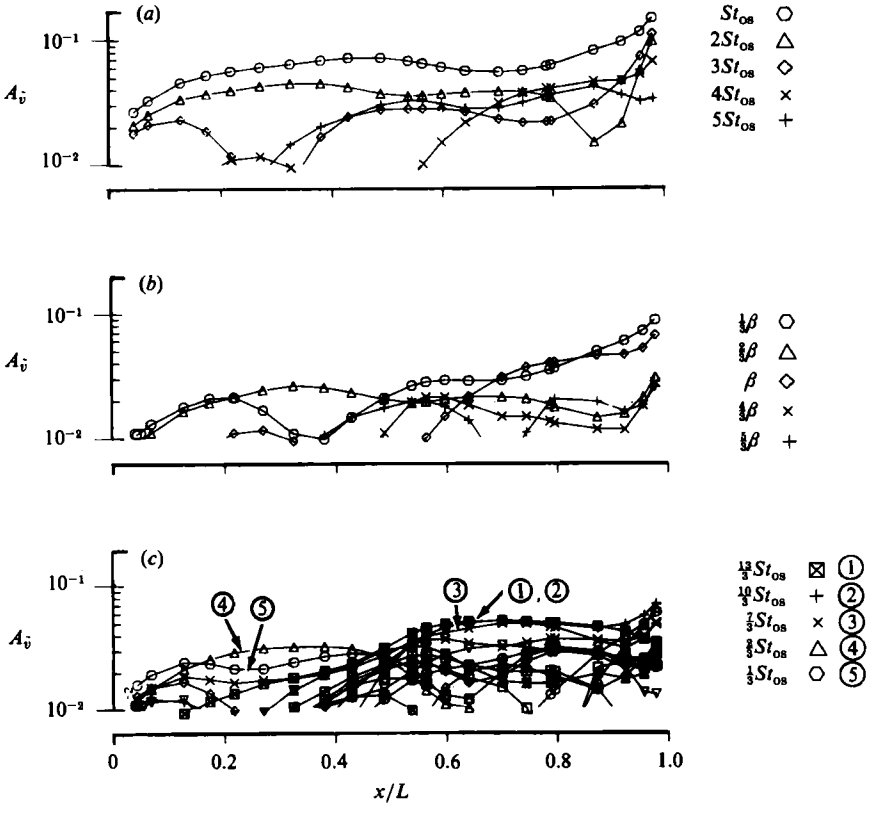

FIGURE 8. Growth of spectral-component amplitudes of the transverse velocity v along the jet centreline ($y = 0$) with $St_{os} = 0.045$, $A = 0.174$: for (*a*) multiples of St_{os}, (*b*) multiples of $\frac{1}{3}\beta$, and (*c*) other frequencies. (Graph vertical ordinates of log type.)

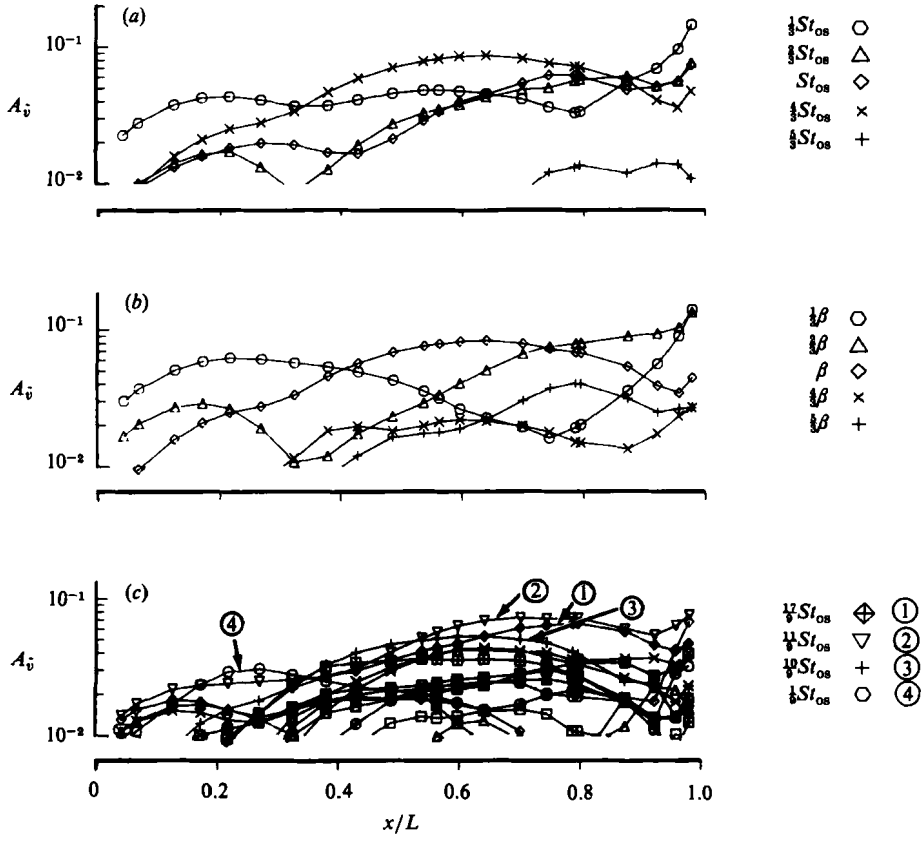

FIGURE 9. As for figure 8 but with $St_{os} = 0.135$, $A = 0.174$ and (*a*) multiples of $\frac{1}{3}St_{os}$.

laboratory by Lucas & Rockwell (1984). The St_{os} curve exhibits an initial growth region from $x/L = 0$ to 0.3, then has a region without growth from $x/L = 0.3$ to 0.8, and finally a secondary growth region from 0.8 to 1.0. This dominance of St_{os} is further evidence that the jet oscillation frequency which was $\frac{1}{3}\beta$ for the unforced case has changed to St_{os} in case (i).

In figure 8(*b*), the component $\frac{1}{3}\beta$ and its multiples are greatly reduced in value from their levels for the unforced case and also significantly smaller than St_{os} and its multiples in figure 8(*a*), providing further evidence that case (i) flow has locked-in to St_{os}.

In the discussion of the flow field for figure 4, it was noticed that during the three periods of forced oscillation, there was a passage of 23 vortices (including vortices d^{I} and d^{II}) which suggests a frequency of $3.83St_{os}$ for vortices shed from either jet shear layer. Figure 8(*c*) shows that the second most dominant component for $0.55 < x/L < 0.9$ is $\frac{13}{3}St_{os}$. Another major component is $4St_{os}$ for x/L in [0.75, 0.90]. These component frequencies are both near $3.84St_{os}$.

Figure 9(*a–c*) shows spectral-component amplitudes for the transverse velocity along the jet centreline ($y = 0$) for case (ii) flow. The dominant components are $\frac{1}{3}\beta$ from $x/L = 0$ to 0.4; β from $x/L = 0.4$ to 0.75 (note that β very nearly equals $\frac{4}{3}St_{os}$); $\frac{2}{3}\beta$ from $x/L = 0.75$ to 0.95; and, $\frac{1}{3}\beta$ and $\frac{1}{3}St_{os}$ from 0.95 to 1.0. These results are in agreement with the discussion of vorticity patterns for case (ii) flow and show that

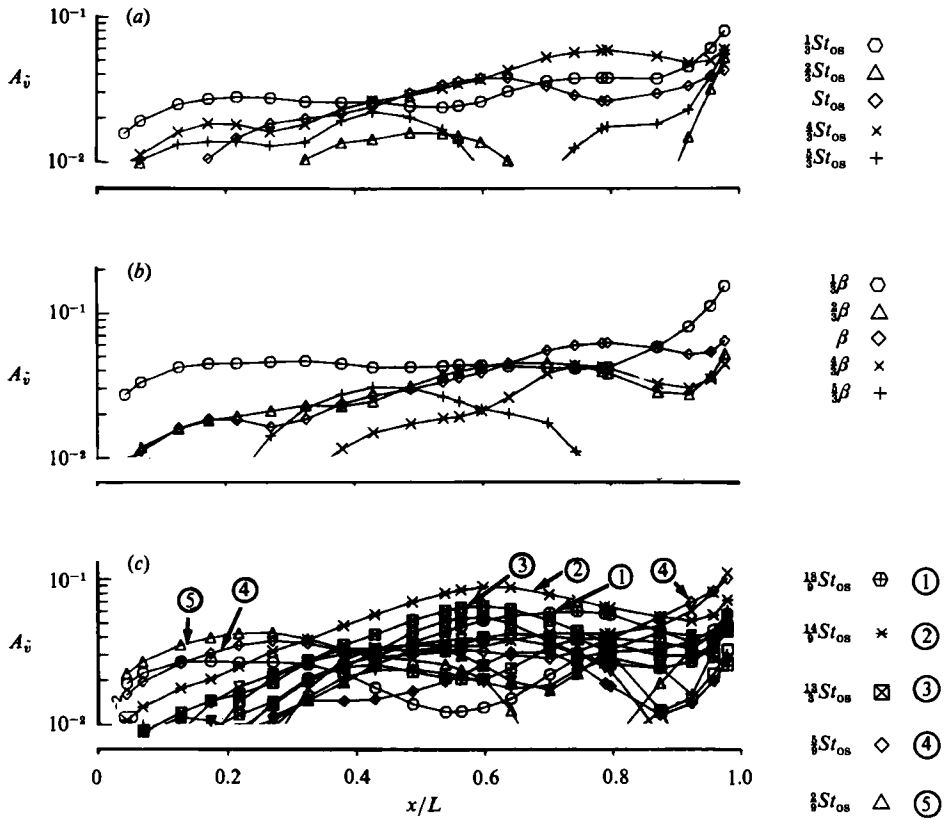

FIGURE 10. As for figure 9 but with $St_{os} = 0.135$, $A = 0.522$.

the dominant frequencies for this case are essentially the same as for the unforced flow.

Figure 10 shows spectral amplitudes for case (iii). Before discussing these results it should be noted that the time interval upon which Fourier analysis was performed was extremely close to $9T$ so that only multiples of $\frac{1}{9}St_{os}$ could be computed and therefore the components for $\frac{1}{2}St_{os}$, $\frac{3}{2}St_{os}$ could not be computed.

The dominant components for case (iii) are $\frac{1}{3}\beta = 0.0585$ (which is approximately equal to $\frac{4}{9}St_{os} = 0.06$) from $x/L = 0$ to 0.4; $\frac{14}{9}St_{os} = 0.21$ from $x/L = 0.4$ to approximately 0.90, and $\frac{1}{3}\beta$ from approximately $x/L = 0.90$ to 1.0. The components $\frac{1}{3}\beta$ and $\frac{14}{9}St_{os}$ are as close in value to $\frac{1}{2}St_{os}$ and $\frac{3}{2}St_{os}$, respectively, as could be obtained. These results are in agreement with the discussion of the vorticity field for case (iii) flow. The component St_{os} near $x/L = 1.0$ is not as large in figure 10 (*a*) as might be expected. Note that the component $\frac{5}{9}St_{os}$ is also prominent near $x/L = 1.0$.

Figure 11 (*a–c*) shows time-history traces of vorticity measured near to and away from the nozzle opening for the three cases. Four traces have a value of essentially zero and were measured at points 1–4 in figure 12 (*a*) having (x, y)-coordinates $(-2.7437, \pm 3.2324)$, and $(-1.7784, \pm 2.2685)$. Four other traces were measured at points 5–8 in figure 12 (*a*). These four locations were symmetrically placed (two on either side of the jet centre) near the outer edge of the jet just downstream of the nozzle opening. All eight points are at the locations where similar records were taken in (O).

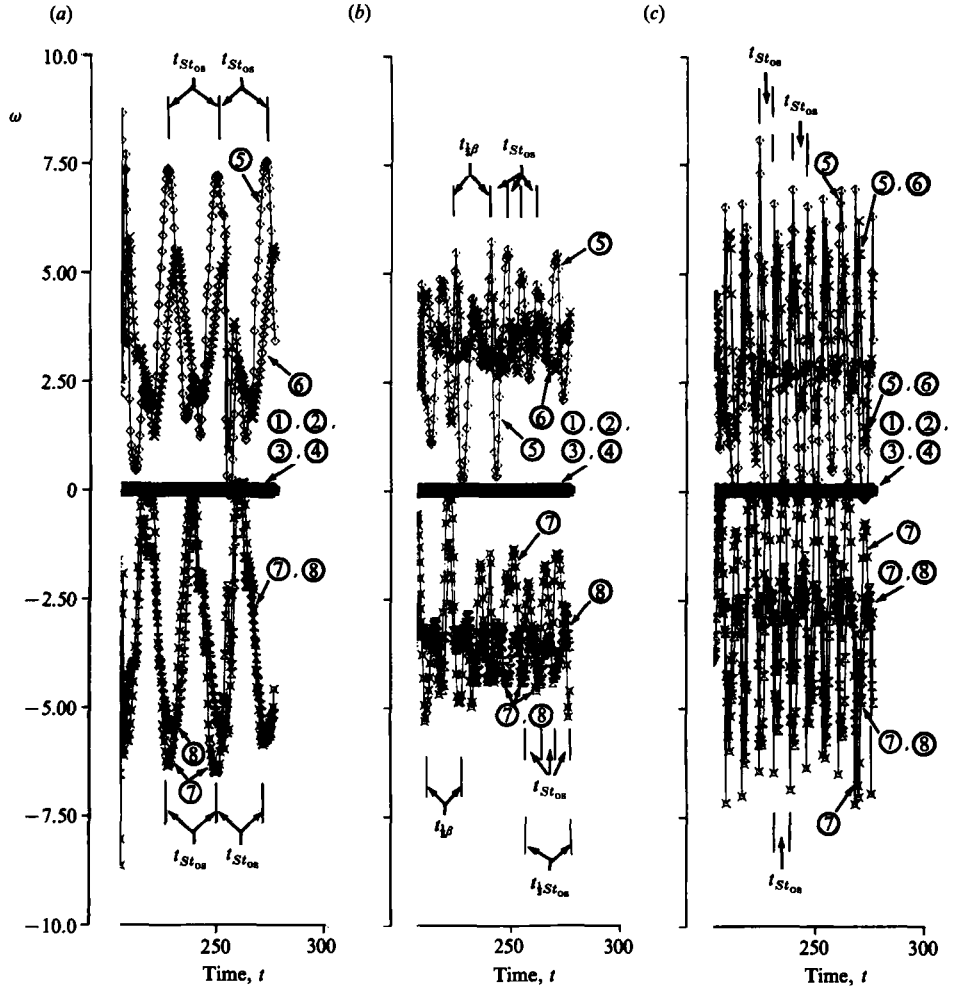

FIGURE 11. Vorticity time histories at selected locations near and away from the nozzle opening for (*a*) $St_{os} = 0.045$, $A = 0.174$, (*b*) $St_{os} = 0.135$, $A = 0.174$, and (*c*) $St_{os} = 0.135$, $A = 0.522$. Point location, (x, y)-coordinates of point location, and plotting symbol for point locations 5–8 are, respectively, 5: (0.6850, 0.4375), ◊ ; 6: (0.7052, 0.3125), × ; 7: (0.6850, −0.4375), ⌑ ; 8: (0.7052, −0.3125), ⧖ .

In figure 11 (*a*), the dominant frequency is St_{os}. This is expected from prior discussion of vorticity and velocity for case (i). For case (i), the two positive traces 5 and 6 (although slightly out of phase with each other) are maximum positive when negative traces 7 and 8 are maximum negative. This clearly shows that the forced symmetric mode is dominant near the channel opening for case (i). This is unlike the unforced case of (O) where the inherent, strongly antisymmetric mode of the jet–edge system dominates. (The period $t_{\frac{1}{3}\beta}$ was the dominant period near the channel opening for the unforced case.)

For cases (ii) and (iii) in figure 11, the dominant frequency is also St_{os}. Case (ii) shows that when positive traces 5 and 6 are minimum, negative traces 7 and 8 are most negative, clearly indicating that the inherent antisymmetric mode is dominant near the channel opening and that the forcing level is not strong enough to overcome

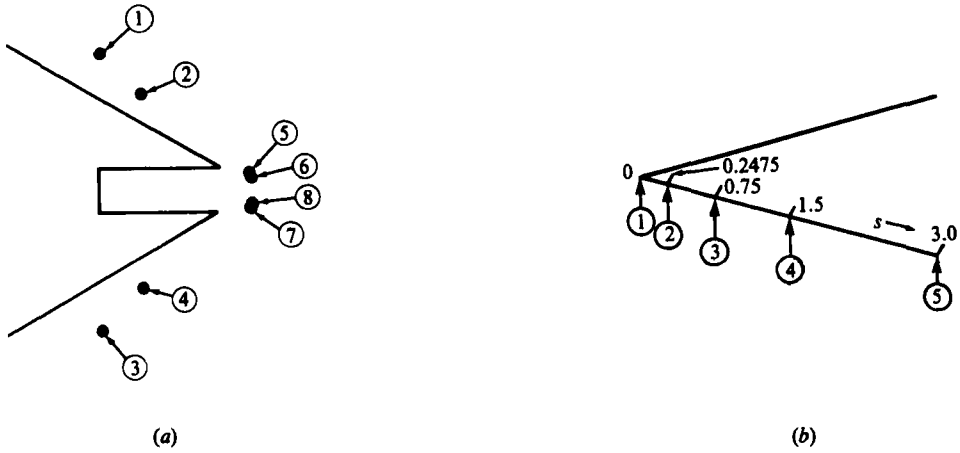

(a) (b)

FIGURE 12. (a) Schematic drawing (drawn to scale) indicating locations of points 1–8 (for figure 11) in the physical domain and (b) locations 1–5 where wedge pressure spectra are taken.

this domination. However, case (iii), like case (i), shows symmetric mode domination. This, when considered along with the magnitude of the vorticity oscillations for cases (i) and (iii) (compared to case (ii)) at the edges of the jet near the channel nozzle, provides further evidence of a lock-in effect to the frequency St_{os} for cases (i) and (iii).

It is interesting to note that the jet oscillation frequencies $\frac{1}{3}\beta$ and $\frac{1}{2}St_{os}$ ($\approx\frac{1}{3}\beta$) for cases (ii) and (iii), respectively, which modulate the jet upstream near the channel nozzle and are the dominant frequencies there for the transverse velocity at the jet centreline (figures 9 and 10), are not the dominant frequencies for the vorticity at the edges of the jet (figure 11*b*, *c*).

3.3. *Numerical spectral results for the wedge pressure*

In figure 12 (*b*) are shown five locations corresponding to the distances 0, 0.2475, 0.75, 1.5 and 3.0, respectively, measured along the lower wedge surface from the wedge tip. Pressure spectra were obtained at these locations, which are the same points for which similar data were presented in (O) for the unforced case. The dominant wedge pressure frequencies for the unforced case were $\frac{1}{3}\beta$, $\frac{2}{3}\beta$ and $\frac{4}{3}\beta$ (with $\frac{2}{3}\beta$ most dominant and being the frequency of wedge impingement).

Figures 13–15 show amplitudes of spectral components for the pressure at the five locations for the three cases. (Spectral analysis for the upper wedge surface is expected to be the same as that of the lower surface.) For all three cases, the dominant component is St_{os} which is to be expected based on prior discussions of the flow visualizations, jet-spectral results, and the fact that in an incompressible fluid the dominant pressure oscillation disturbance for the incoming flow is transmitted immediately to the surrounding flow.

For case (i), (figure 13) it was found that minima in the pressure–time traces near the tip occur when a jet vortex is passing underneath, i.e. at times $t = 216.4$, 240.4, 264.4 and at 256.4 (the largest minimum). The maximum in the pressure traces occurs at $t = 250.0$ when no jet vortex is underneath the wedge (see figure 4).

In figure 14, for case (ii) which has relatively weak forcing, the components β, $\frac{2}{3}\beta$, $\frac{1}{3}\beta$ are not prominent despite the fact that this might be expected from prior discussion. Instead, the components St_{os} and $\frac{1}{3}St_{os}$ are most dominant.

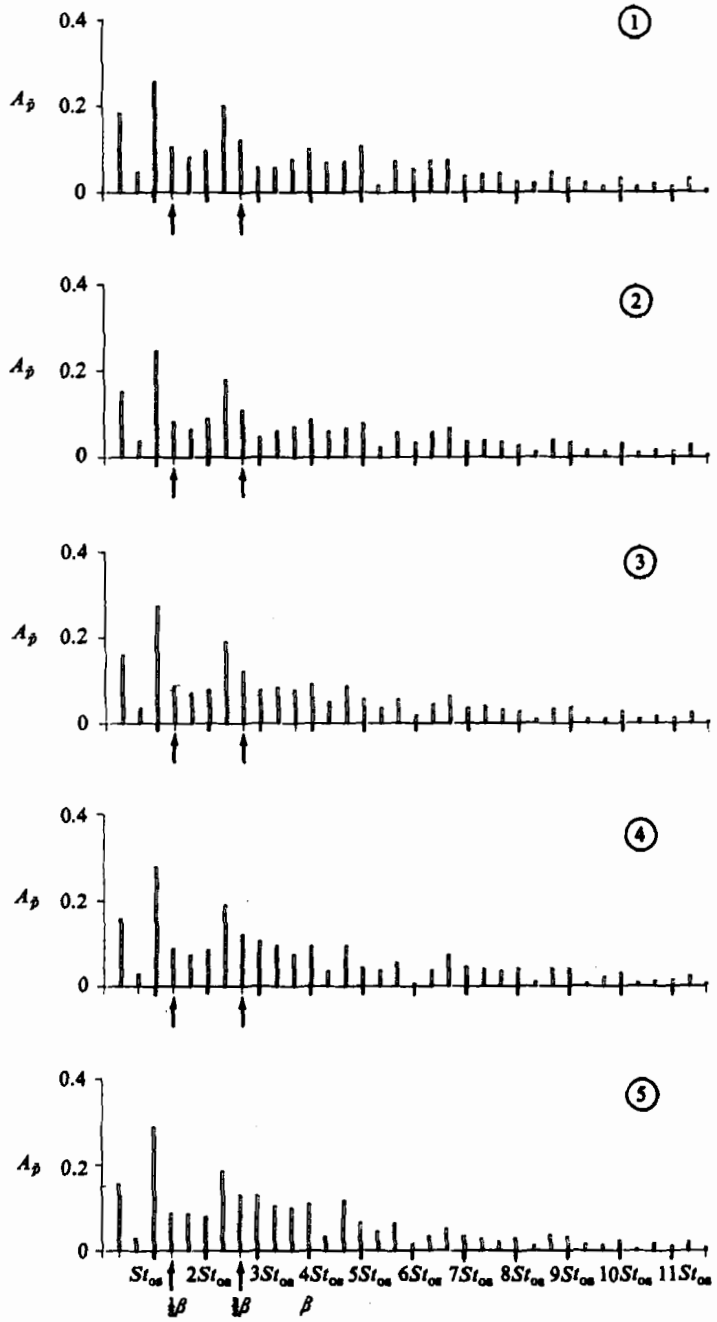

FIGURE 13. Spectral-component amplitudes for the wedge pressure at the five locations of figure 12(*b*). $St_{os} = 0.045$, $A = 0.174$.

In figure 15, for case (iii), the component St_{os} is huge. It was found that minima in the pressure traces occur at times of jet impingement that have a period equal to the period of the forced oscillation. The greatest minima occur at $t = 245.6$ and 268.4 (see figure 6).

The same comments apply to the wedge pressure spectral components as were

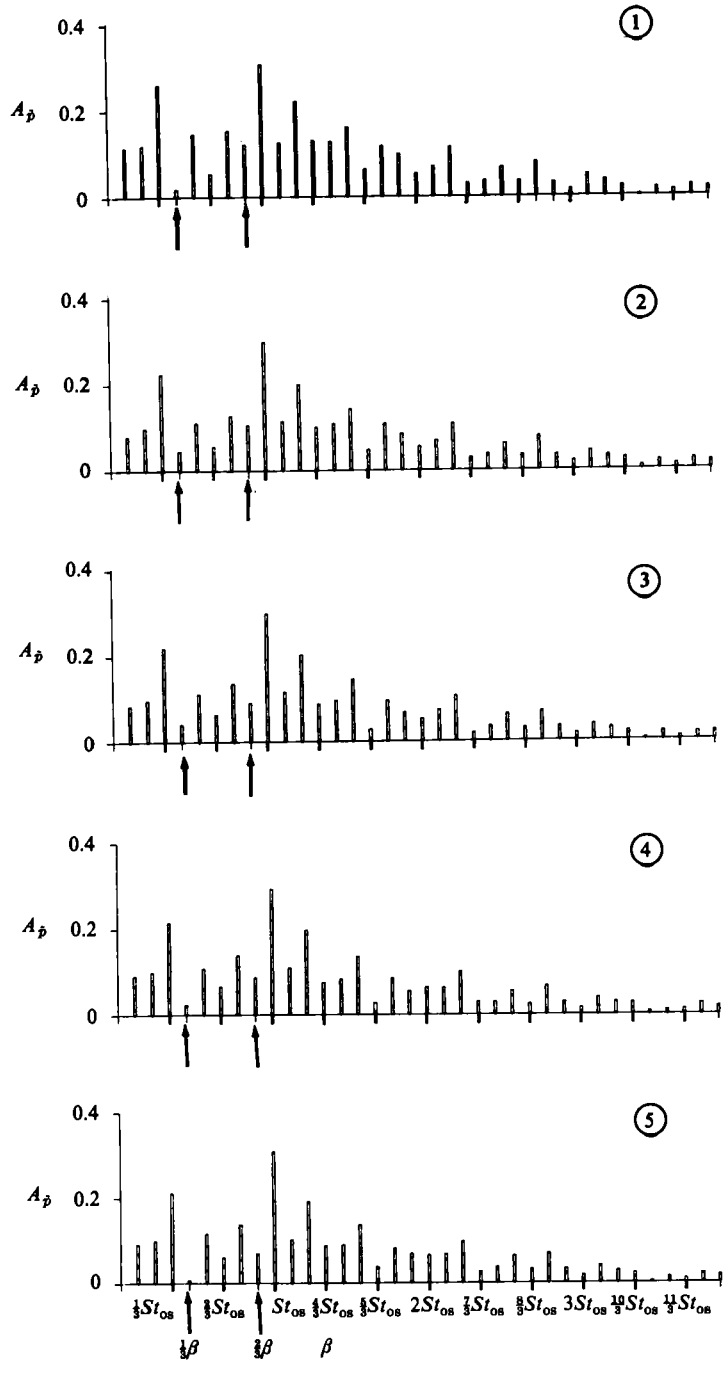

FIGURE 14. As for figure 13 but with $St_{os} = 0.135$, $A = 0.174$.

previously made for the jet spectral components concerning the unavailability of many computed flow cycles for the three cases (i), (ii) and (iii) which would have permitted better resolution by Fourier analysis of the increased number of spectral components due to the mechanical forcing.

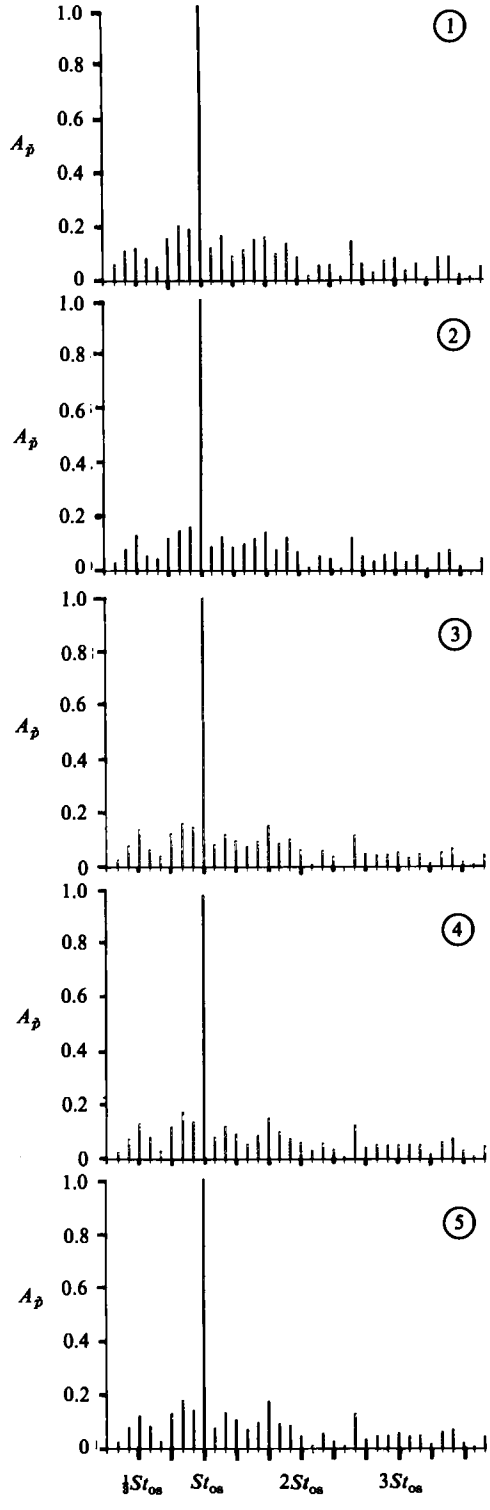

FIGURE 15. As for figure 13 but with $St_{os} = 0.135$, $A = 0.522$.

4. Conclusions

Numerical calculations have been performed to study the effect of forced, symmetric, longitudinal, incoming flow oscillations on the inherent, strongly antisymmetrical oscillations of the edgetone flow. These forced incoming flow oscillations are, in themselves, an analytic solution to the time-dependent Navier–Stokes equations. The edgetone flow chosen to be forced is at Reynolds number 450 (based on the channel width and average velocity of the unforced incoming Couette flow) and was computed previously in Ohring (1986) (denoted there as $Re = 450$ (from 650) and in the present paper as the unforced case). This unforced edgetone flow has two major naturally occurring frequencies: $\frac{1}{3}\beta = 0.0585$ representing the frequency of one complete jet oscillation and $\beta = 0.1754$ representing the frequency of vortices shed from either jet shear layer during a complete jet oscillation. These two naturally occurring frequencies were also found experimentally in the laboratory by Lucas & Rockwell (1984).

Three cases with forcing were studied in the present paper. Case (i) had a forced incoming flow oscillation frequency St_{os} which was 23.08 % less than $\frac{1}{3}\beta$ and whose maximum (or minimum) incoming velocity at $y = 0$ (the channel centre) was 42.05 % greater (or less) than the maximum steady, incoming Couette flow velocity at $y = 0$. Cases (ii) and (iii) had a forced incoming flow oscillation frequency 23.08 % less than β. Case (ii) had a maximum (or minimum) incoming velocity at $y = 0$ that was 13.65 % greater (or less) than the maximum, steady incoming Couette flow velocity at $y = 0$ while the corresponding percentage for case (iii) was 40.96 %.

Results for case (i) showed that the naturally occurring jet oscillation frequency $\frac{1}{3}\beta$ was changed and locked-in to the forced frequency St_{os}. In addition, it was found that $\frac{1}{3}\beta$ and its integer multiples were significantly diminished and that the dominant frequency of the flow was St_{os}, providing further evidence that the flow had locked-in to St_{os}.

Case (ii) results indicate a transition from the unforced case toward case (iii) flow. Case (ii) flow is similar to the unforced case in that: (*a*) case (ii) has dominant frequencies β, $\frac{1}{3}\beta$, $\frac{2}{3}\beta$; and, (*b*) impingements occur with frequency $\frac{2}{3}\beta$. Case (ii) flow differs from the unforced case in the following important respects: (*a*) jet shear-layer vortices are stronger and are shed further upstream nearer to the channel nozzle; (*b*) a swaying jet is not as easily discernible as the length of the jet stem varies considerably at different times; and, (*c*) β is a more dominant frequency.

Case (iii) results show that: (*a*) the entire jet appears to be oscillating with a frequency $\frac{1}{2}St_{os}$ during a time period shorter than that for the unforced case; (*b*) the jet is impinging at the wedge with frequency St_{os}; and, (*c*) three vortices are shed from each side of the jet during a jet oscillation which yields another dominant frequency $\frac{3}{2}St_{os}$. Case (iii) flow has locked-in to the dominant frequencies $\frac{1}{2}St_{os}$, St_{os} and $\frac{3}{2}St_{os}$.

The following statements apply to cases (i)–(iii) based on the results obtained in this paper:

1. The high forcing level of cases (i) and (iii) caused: (*a*) lock-in of the jet–edge system to the forcing frequency St_{os} (at both the lower and higher forcing frequencies of cases (i) and (iii), respectively), and (*b*) the domination of the forced symmetric mode over the inherent, strongly antisymmetrical oscillations of the jet–edge system near the channel opening with the symmetric mode domination extending a considerable distance downstream of the channel opening for case (iii). For the relatively low level of forcing used for case (ii), lock-in of the jet–edge system to the

higher forcing frequency of case (ii) is not achieved and no forced symmetric mode domination exists.

2. Although there is considerable variation of the jet structure among cases (i)–(iii), an oscillating or 'flapping' jet is preserved in the jet–edge system despite the forcing. Comparisons of the forced cases (i)–(iii) with each other and with the unforced case with regard to earlier (further upstream) vortex formation, pairing and amalgamation show results analogous to those shown from comparisons of forced cases with each other in Ho & Huerre (1984) where the forcing was applied to a free shear layer emanating from a splitter plate.

3. For all three cases, the forcing frequency St_{os} is the dominant component for pressure at the wedge and jet edge vorticity near the channel nozzle. The wedge pressure component St_{os} for case (iii) is huge with the forced frequency St_{os} also the frequency of impingement.

4. For all three cases, the additional flow energy provided by the forced, mechanical, longitudinal oscillations resulted in a significant increase in the number of non-zero spectral components beyond that for the corresponding unforced edgetone flow.

This work was supported by the Independent Research Program at the David W. Taylor Naval Ship Research and Development Center. The author wishes to thank Dr Hans Lugt of the David W. Taylor Naval Ship Research and Development Center, Bethesda, Maryland, for suggesting this study and for valuable discussions and comments.

REFERENCES

Ho, C. & Huerre, P. 1984 Perturbed free shear layers. *Ann. Rev. Fluid Mech.* **16**, 365–424.

Lucas, M. & Rockwell, D. 1984 Self-excited jet: upstream modulation and multiple frequencies. *J. Fluid Mech.* **147**, 333–352.

Ohring, S. 1986 Calculations of self-excited impinging jet flow. *J. Fluid Mech.* **163**, 69–98.

Powell, A. 1961 On the edgetone. *J. Acoust. Soc. Am.* **33**, 395–409.

Rockwell, D. 1971 The macroscopic nature of jet flows subjected to small amplitude periodic disturbances. *Chem. Engng Symp. Series*, vol. **67**, no. 109, pp. 99–107.

Schlichting, H. 1968 *Boundary-Layer Theory*. McGraw-Hill.

Staubli, T. & Rockwell, D. 1987 Interaction of an unstable planar jet with an oscillating leading edge. *J. Fluid Mech.* **176**, 135–167.